Journal of Instrumentation

PAPER

Improvement of the CGEM detector simulation with cosmic-rays

To cite this article: X.L. Lu *et al* 2023 *JINST* **18** P05027

Jinst

Published by IOP Publishing for Sissa Medialab

Received: *March 21, 2023*
Accepted: *April 20, 2023*
Published: *May 22, 2023*

Improvement of the CGEM detector simulation with cosmic-rays

X.L. Lu,[a,b] **L.L. Wang,**[a,b,*] **H. Zhou,**[c] **Z.H. Zhang,**[a,b] **L.H. Wu,**[a,b] **H.M. Liu,**[a,b] **A. Amoroso,**[d,e] **R. Baldini Ferroli,**[f] **I. Balossino,**[a,g] **M. Bertani,**[f] **D. Bettoni,**[g] **F. Bianchi,**[d,e] **A. Bortone,**[d,e] **G. Cibinetto,**[g] **A. Cotta Ramusino,**[g] **F. Cossio,**[e] **G. Cotto,**[d,e] **M.Y. Dong,**[a,b] **M. Da Rocha Rolo,**[e] **F. De Mori,**[d,e] **M. Destefanis,**[d,e] **J. Dong,**[a] **F. Evangelisti,**[h,g] **R. Farinelli,**[g] **L. Fava,**[i,e] **G. Felici,**[f] **I. Garzia,**[h,g] **M. Gatta,**[f] **G. Giraudo,**[e] **S. Gramigna,**[h,g] **S. Garbolino,**[e] **M. Greco,**[d,e] **A.Q. Guo,**[j,b] **Z. Huang,**[k] **Y.R. Hou,**[b] **W. Imoehl,**[l] **L. Lavezzi,**[d,e] **M. Maggiora,**[d,e] **F.M. Melendi,**[h,g] **R. Malaguti,**[g] **A. Mangoni,**[m,f] **S. Marcello,**[d,e] **M. Melchiorri,**[g] **G. Mezzadri,**[g] **R.E. Mitchell,**[l] **Q. Ouyang,**[a,b] **S. Pacetti,**[m,f] **P. Patteri,**[f] **A. Rivetti,**[e] **R.S. Shi,**[a,b] **M. Scodeggio,**[h,g] **S. Sosio,**[d,e] **S. Spataro,**[d,e] **B.L. Wang,**[b] **H.P. Wang,**[a,b] **Y. Zhang**[a,b] **and J.Y. Zhao**[a,b]

[a] *Institute of High Energy Physics, Chinese Academy of Sciences, Beijing 100049, People's Republic of China*
[b] *University of Chinese Academy of Sciences, Beijing 100049, People's Republic of China*
[c] *University of Science and Technology of China, Hefei 230026, People's Republic of China*
[d] *Università di Torino, Dipartimento di Fisica, via P. Giuria 1, Torino 10125, Italy*
[e] *INFN, Sezione di Torino, via P. Giuria 1, Torino 10125, Italy*
[f] *INFN, Laboratori Nazionali di Frascati, via E. Fermi 40, Frascati 00044, Italy*
[g] *INFN, Sezione di Ferrara, via G. Saragat 1, Ferrara 44122, Italy*
[h] *Università di Ferrara, Dipartimento di Fisica e Scienze della Terra, via G. Saragat 1, Ferrara 44122, Italy*
[i] *Università del Piemonte Orientale, Dipartimento di Scienza e Innovazione Tecnologica, Viale Teresa Michel 11, Alessandria 15121, Italy*
[j] *Institute of Modern Physics, Chinese Academy of Sciences, Lanzhou 730000, People's Republic of China*

[*] Corresponding author.

https://doi.org/10.1088/1748-0221/18/05/P05027

2023 JINST 18 P05027

[k] *Peking University,*
Beijing 100871, People's Republic of China
[l] *Indiana University,*
Bloomington, Indiana 47405, U.S.A.
[m] *Università di Perugia, Dipartimento di Fisica e Geologia,*
via A. Pascoli, Perugia 06123, Italy

E-mail: llwang@ihep.ac.cn

Abstract: A Cylindrical Gas Electron Multiplier (CGEM) is under construction for the upgrade of the BESIII inner tracker. A preliminary simulation of the CGEM signal before the frond-end electronics has been worked out by making some sampling models from the beforehand Garfield++ simulation. The electronics response functions are implemented making the simulation of CGEM more complete. By comparing the cosmic-ray data acquired by two layers of CGEM and the simulation, the micro-sector effect is simulated and some key parameters in the sampling models are fine tuned in this order: gain, charge sharing, charge fluctuation and electron diffusion. A general agreement is achieved between the cosmic-ray data and the simulation with these improvements.

Keywords: Micropattern gaseous detectors (MSGC, GEM, THGEM, RETHGEM, MHSP, MICROPIC, MICROMEGAS, InGrid, etc); Simulation methods and programs

2023 JINST 18 P05027

Contents

2023 JINST 18 P05027

1 Introduction

The Beijing Spectrometer III (BESIII) [1] is a multiple-purpose detector operating at the upgraded Beijing Electron Positron Collider (BEPCII) [2], and designed to study physics in the tau-charm energy region, including light hadron spectroscopy, charmed mesons, charmonia, exotic states, τ lepton, and so on [3]. BESIII is described in detail in ref. [1], and it consists of a Multilayer Drift Chamber (MDC) filled with a helium-based gas, an electromagnetic calorimeter made of CsI(Tl) crystals, time-of-flight (TOF) counters made of plastic scintillators, a muon system made of resistive plate chambers, and a superconducting magnet providing a field of 1 Tesla. MDC is the key detector of BESIII to measure the trajectory of charged particles and is composed of two parts: the inner and outer chambers. After many years of operation, the inner chamber, which surrounds closely the electron and positron beams, has been severely affected by radiation and has suffered from ageing problems such as reduced gas gain, degenerative spatial resolution, and increased dark current [4]. A Cylindrical Gas Electron Multiplier Inner Tracker (CGEM-IT) [5] is chosen as a solution for the upgrade of the BESIII inner chamber, since GEM has as advantages of stable operation at high count rates, good spatial resolution, and radiation resistance [6]. The CGEM-IT is composed of three coaxial layers of cylindrical triple-GEMs, operating in an $Ar + iC_4H_{10}$ (90 : 10) gas mixture

with field and gain optimized to minimize the spatial resolution. Two layers of CGEM have been constructed and the third one is under construction [7].

To perform Monte-Carlo studies and to prepare for the CGEM-IT commissioning at BESIII, the offline software development is also in progress including simulation, reconstruction, calibration and alignment. Within the framework of the BESIII offline software system (BOSS) [8], the description of the CGEM detector as well as the supplementary parts, like the support structure and cables, are implemented with GEANT4 [9]. A digitization model [10] is also developed to simulate the signal of firing strips of the CGEM for charged particles crossing the detector. However, a more detailed simulation including the electronics response and the effect from the micro-sector segmentation of the GEM foils is still missing; the initial parameters of the digitization model are obtained from the Garfield++ simulations [10] without any test with data. Additional implementations and fine tuning based on data are needed to realize a good simulation of CGEM detector in practice. A cosmic-ray setup with two out of three layers of CGEM is in operation in Beijing since January 2020, and it provides cosmic-ray data which can be used as a reference to improve the CGEM simulation.

In this paper, we describe the improvements of the simulation of the CGEM-IT with the cosmic-ray data. The following information is presented: the cosmic-ray setup with CGEM, the reconstruction of cosmic-ray data, the simulation of cosmic-rays, the further implementation of the digitization model taking into account the electronics response and the effects of the micro-sectors, the fine tuning of the digitization model including gain, charge sharing, charge fluctuation, electron diffusion, and the comparison of the cosmic-ray data and the simulation.

2 Cosmic-ray setup

The scheme of the cosmic-ray setup, using two layers of CGEM, is shown in the left plot of figure 1. Two layers of scintillator bars, which are placed above and below the CGEM detectors, are used as a trigger system. Typically, four hits for each cosmic-ray are obtained by the two layers of detectors. If the detectors are divided into four half-layers, layer 2 top, layer 1 top, layer 1 bottom, and layer 2 bottom, there is one hit in each half-layer expected from a cosmic-ray. The inner radii of the two CGEMs are 76.9 mm and 119.4 mm, and the active lengths 532 mm and 690 mm, respectively. As shown in the right plot of figure 1, each layer is composed of a cathode, three GEM foils (GEM1, GEM2 and GEM3), and an anode, with four gaps between them — a drift gap, two transfer gaps and an induction gap. Each anode provides two dimensional readout with X-view strips (X-strips) which are axial and V-view strips (V-strips) which have a layer dependent stereo angle with respect to the X-ones. The strip pitch is 660 µm for both views and all layers. The signal from the strip is amplified and digitized by a frond-end ASIC, Torino Integrated GEM Electronics for Readout (TIGER) [11], which can provide charge and time measurements. The outputs of TIGERs are collected by GEM Read Out Cards, the data packets of triggered events are built with GEM Data Concentrators and finally sent to the BESIII data acquisition system for storage [11].

3 Cosmic-ray data reconstruction

The data packets from the cosmic-ray setup are decoded and transferred into the BOSS framework for offline reconstruction, selection and analysis. First, the signals from the two layers of CGEM

2023 JINST 18 P05027

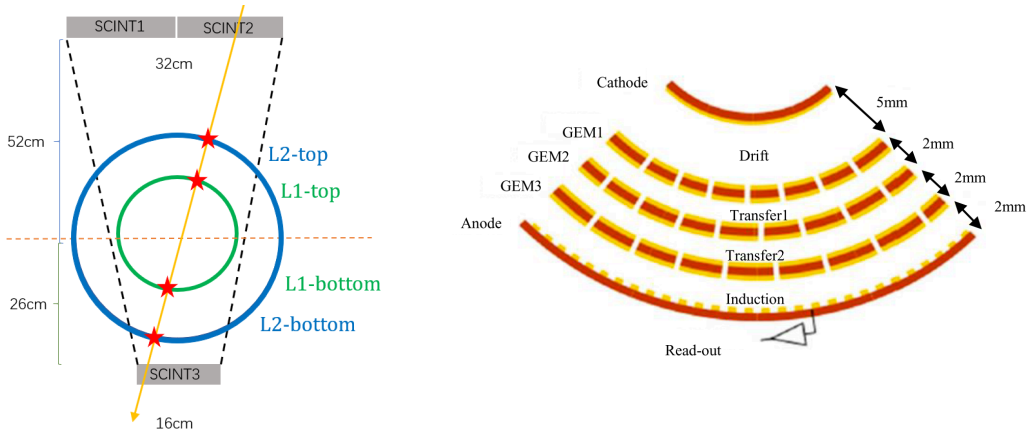

Figure 1. Left: a scheme of the cosmic-ray setup consisting of two layers of CGEM detectors (two circles) and scintillator bars (grey boxes), where the orange line with an arrow represents a cosmic-ray and the four red stars the hits from the cosmic-ray. Right: a scheme of the structure of each CGEM layer.

detectors are processed to make clusters. Then clusters are used to reconstruct cosmic-rays. The procedure is described in detail in the following subsections.

3.1 Cluster reconstruction

Each set of contiguous firing strips is reconstructed as a single cluster. The clustering is applied for both views. The one-dimensional-clusters (1D-cluster) with X-strips (or V-strips) are called X-clusters (or V-clusters). Since each strip provides a charge and a time measurement at the same time, the position of a 1D-cluster can be reconstructed with two methods, the Charge Centroid (CC) and the micro-Time Projection Chamber (μTPC) [12]. The CC method averages the strip positions in the cluster using their charge as weight. This method is straightforward, robust and gives better resolution for tracks with a small incident angle. The μTPC method calculates for each strip the perpendicular distance of the primary ionization from the readout plane using the time information. It then performs a linear fit on the primary ionization points reconstructed in the drift gap to extract the position of the cluster in the middle of the gap. This method provides better resolution for tracks with a large incident angle but needs a thorough calibration of time measurements. In this study, the CC method is used. A combination of a X-cluster and a V-clusters on the same readout plane is called a two-dimensional-cluster (2D-cluster).

3.2 Cosmic-ray selection

The four hits shown in the left plot of figure 1 for a cosmic-ray correspond to four 2D-clusters, one on each half-layer. Since the measurement can be affected by spurious clusters induced by noise, an algorithm is developed to select signal clusters from cosmic-rays. The 2D-clusters are required in the geometry acceptance of the trigger system. At most the three 2D-clusters with the largest charge on each half-layer are selected. All the combinations of four 2D-clusters with one on each half-layer are fitted to a three dimensional straight line with the least square method. The combination with the smallest χ^2 of the fit is selected for each event and kept as a cosmic-ray candidate, with $\chi^2 < 80$. Finally, about 141 thousand cosmic-ray candidates are obtained from the data. The alignment of

2023 JINST 18 P05027

the detectors in the cosmic-ray setup is performed [13], and the alignment parameters are used in this study. The 2D-cluster position maps for the cosmic-ray candidates are shown in figure 2, and the external outlines correspond to the geometry acceptance of the trigger system.

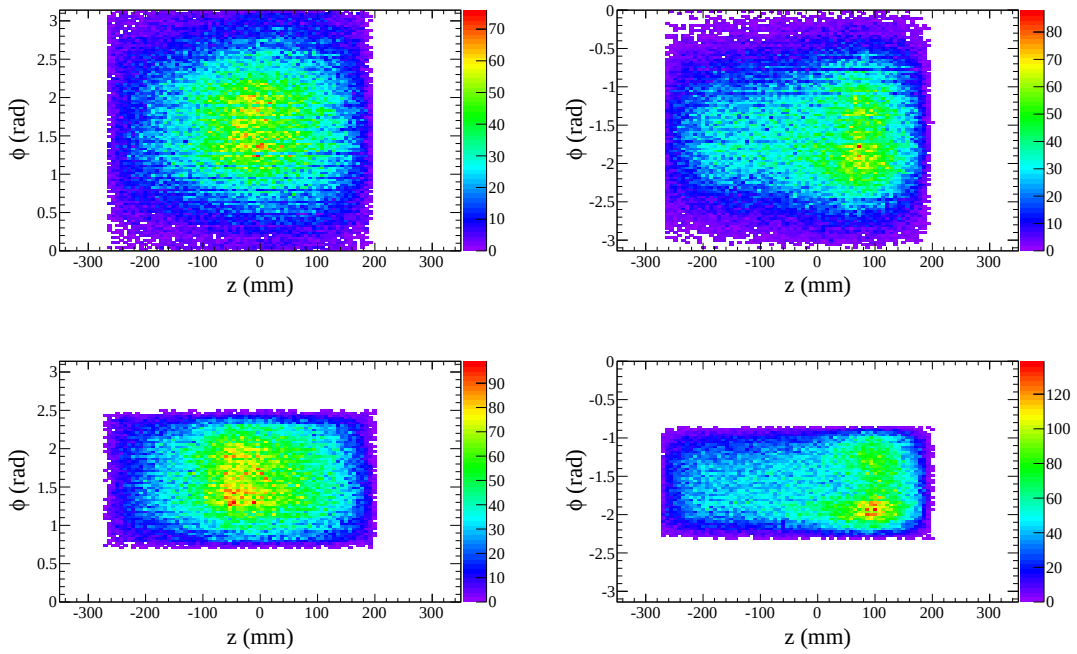

Figure 2. The 2D-cluster position distributions for the cosmic-ray candidates on layer 1 top (top left), layer 1 bottom (top right), layer 2 top (bottom left) and layer 2 bottom (bottom right).

4 Cosmic-ray simulation

Cosmic-ray Monte-Carlo (MC) samples with a statistics about 2.6 times the one of the data sample are generated hitting the plane of the upper scintillator bars, according to the differential flux of athmospheric muons at sea level [14, 15].

The trajectory of cosmic-rays in CGEM is simulated with GEANT4. The electrons produced in the ionization of the gas by the cosmic-ray crossing the drift gap of a CGEM detector are generated by the Heed package [16]. The ionization electrons drift from the drift gap to the induction gap, and are multiplied as crossing the triple GEM foils. The number, position and time of the electrons are simulated in cascade by the sampling models built by parameterizations of the distributions of electrons from beforehand Garfield++ simulations. Also, the induced currents of the nearby strips are simulated with beforehand Garfield++ for single electrons in the induction gap, and this information is stored and used in the digitization for each electron coming from the multiplication. Then the total number of firing strips and their induced currents are given by the sum of the contributions from all the multiplied electrons in the induction gap. The sampling model and the simulation of the induction response are described in detail in ref. [10]. The induced current on each strip is processed by the TIGER to perform charge and time measurements. The simulation of the electronics response, as a part of this work, is described in section 5.1.

2023 JINST 18 P05027

The same cluster reconstruction and cosmic-ray selection are applied to both data and MC samples, except for the alignment since the ideal geometry is used for MC. The 2D-cluster position distributions for the simulated cosmic-ray candidates are shown in figure 3. In comparison, the distribution from data (figure 2) shows a higher concentration on the forward part ($z > 0$) especially for the bottom half-layers. To take into account this experimental hit distribution, the clusters of MC cosmic-rays are always weighted in the following studies with the ratio of the 2D-cluster position distributions of data over MC on the each half-layer.

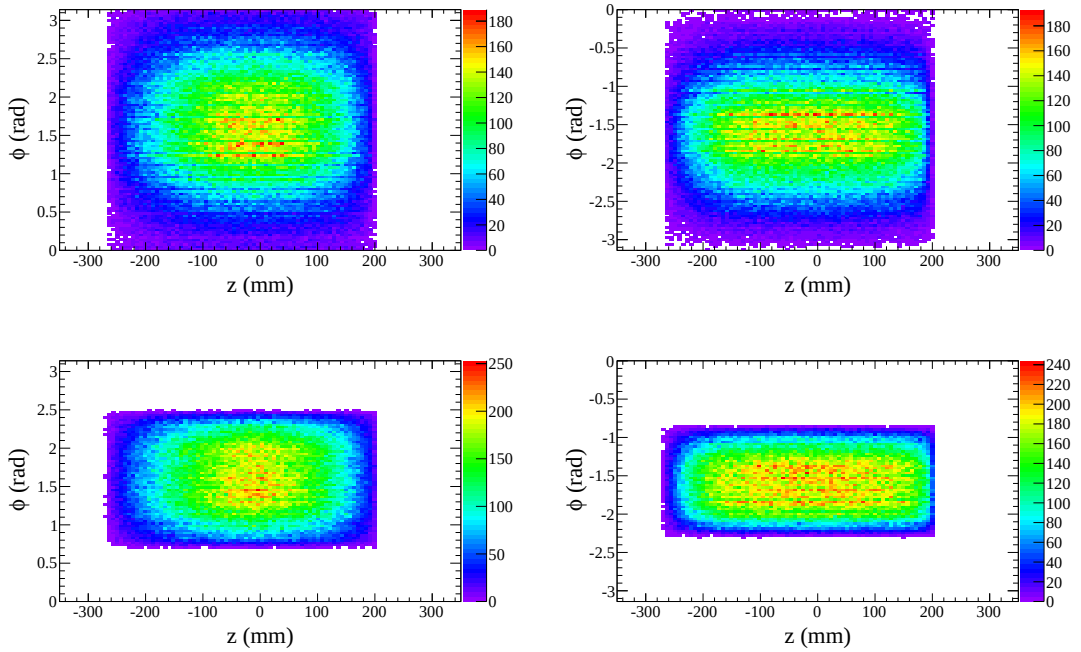

Figure 3. The 2D-cluster position distributions for the MC cosmic-ray candidates on layer 1 top (top left), layer 1 bottom (top right), layer 2 top (bottom left) and layer 2 bottom (bottom right).

5 Further implementation of the digitization model

The digitization model is improved with respect to the original one [10] by some further implementations, including the simulation of the electronic response and also of the micro-sector segmentation, as it follows.

5.1 Simulation of electronics response

The main signal processing functions in electronics, which need to be simulated, are those reproducing the TIGER response for time and charge measurements. The TIGER [11] has two measurement branches, a fast one for time, a slow one for charge, which are called T-branch and E-branch, respectively. Both branches have a discriminator allowing threshold setting independently for each branch and each channel. The time of the threshold crossing in T-branch is taken as the time measurement and the trigger for E-branch. The charge measurement in E-branch has two modes: Time-Over-Threshold and Sample-and-Hold [11], where the latter is used in the cosmic-ray data

taking. The final measured charge is converted from the E-branch output by a linear calibration curve. Only signals crossing threshold in both branches are kept.

To simulate the signal shaping, response functions are estimated for both branches. The induced signal of the strip is convoluted with the response function to simulate the signal after shaping in each branch. The time and charge measurement logic introduced previously is implemented in simulation including the calibration curve. The channel and branch dependent thresholds are set in simulation according to the values set during the cosmic-ray data taking. The saturation effect in charge measurement is also included. Figure 4 shows the charge versus the X-strip number on layer 1 top for the data and the MC after the simulation of the electronics, and a general agreement between them on the thresholds and saturation is achieved. Hereafter the layer 1 top is always taken as an example for the demonstration in the following studies, since the other three half-layers provide similar results.

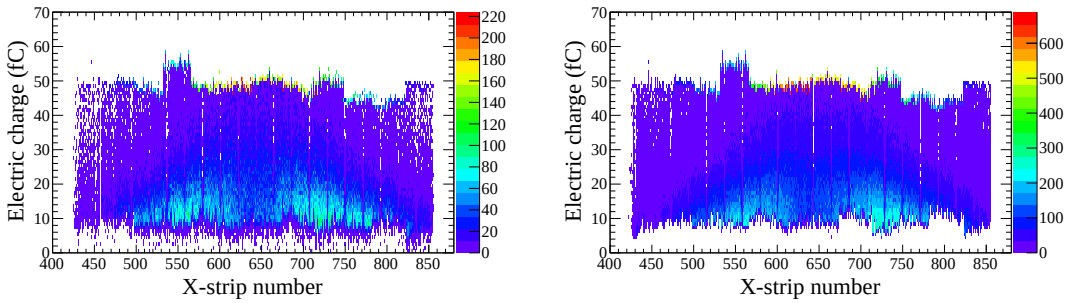

Figure 4. Charge versus X-strip number distributions on layer 1 top for the data (left) and the MC (right).

5.2 Micro-sector effect

Some evenly spaced vertical crack lines are visible in the charge versus X-strip number plot for data (figure 4 left). This is called the "micro-sector" effect, and it is caused by the design of the GEM foils. Indeed, both sides of each GEM foil have a copper plane; one plane is segmented into macro-sectors, and the other into micro-sectors [11]. These sectors work as electrodes providing strong electrical fields in the holes of GEM foil for electron multiplication. The sectors are separated by small slits which affect the multiplication of the nearby electrons. In order to reproduce this effect, in simulation the electrons from multiplication hitting the space around the slits are discarded. As can be seen in the right plot of figure 4, the simulation reproduces consistently these regions.

6 Fine tuning of digitization model

By including the additional implementations described in the previous section, the CGEM digitization model is quite complete. However, the parameters extracted from Garfield++ simulations need a fine tuning to better match simulated and experimental results. The cluster charge, cluster charge sharing between two views and cluster size distributions are the measurements which can be compared between data and MC. The most relevant parameters in the digitization model are identified and their tuning is organized in this order: gain, charge sharing, charge fluctuation, and

2023 JINST 18 P05027

electron diffusion, to reduce the correlation between the tuning of different parameters. As long as one tuning is performed, the tuned factor is always applied thereafter. The four half-layers of the CGEM detectors used in the cosmic-ray setup are separated in the tuning to take into account the possible difference between them.

6.1 Gain

The electron multiplication when going through GEM foils is simulated in the digitization model [10] by sampling with the Polya distribution [17]

$$P(G) = C_0 \frac{(1+\theta)^{1+\theta}}{\Gamma(1+\theta)} \left(\frac{G}{G_0}\right)^{\theta} \exp\left[-(1+\theta)\frac{G}{G_0}\right], \tag{6.1}$$

where C_0 is a constant, G is the gain for a single electron, G_0 is the mean gain, and θ is a parameter which determines the variance of the distribution. The 2D-cluster charge distributions for MC do not depend strongly on charge sharing, charge fluctuation and electron diffusion, while mainly depend on the parameter G_0. So, the mean gain in the digitization model G_0 is tuned firstly by multiplying it with a scaling factor. The 2D-cluster charge distributions for the data and the MC with different gain scaling factors on layer 1 top are shown in the left plot of figure 5. The consistency level of the 2D-cluster charge distributions between the data and the MC is evaluated by a χ^2 test [18–20]. The χ^2/ndf between data and MC for different gain scaling factors are shown in the right plot of figure 5. Gain scaling factors 1.64, 1.64, 1.64, and 1.62 minimize the χ^2/ndf of 2D-cluster charge distributions between data and MC on layer 1 top, layer 1 bottom, layer 2 top, and layer 2 bottom, respectively. The gain scaling factors for the four half-layers are quite consistent between each other.

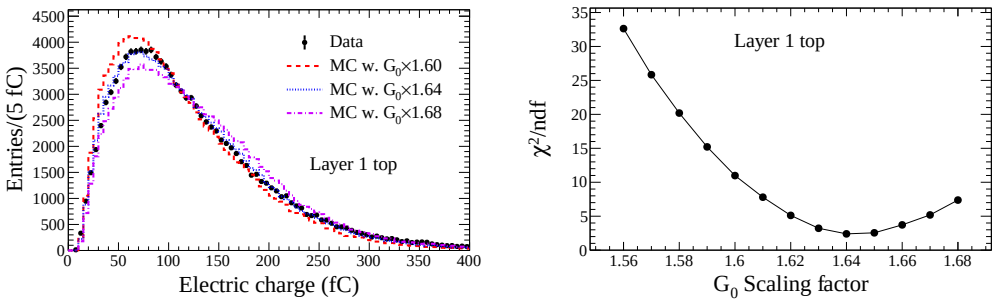

Figure 5. Left: 2D-cluster charge distributions for data and MC on layer 1 top. Right: χ^2/ndf of the 2D-cluster charge distributions between data and MC as a function of G_0 scaling factor on layer 1 top.

6.2 Charge sharing

In each 2D-cluster, the charge sharing between the V-cluster and the X-cluster (denoted as Q_V/Q_X) can be calculated for both data and MC. It is strongly connected to the charge sharing at induction between the two views for individual electrons in the simulation. The charge sharing (Q_V/Q_X) in simulation is tuned by multiplying the fraction of charge in X-view (denoted as f_{q_X}) at induction with a common scaling factor.

2023 JINST 18 P05027

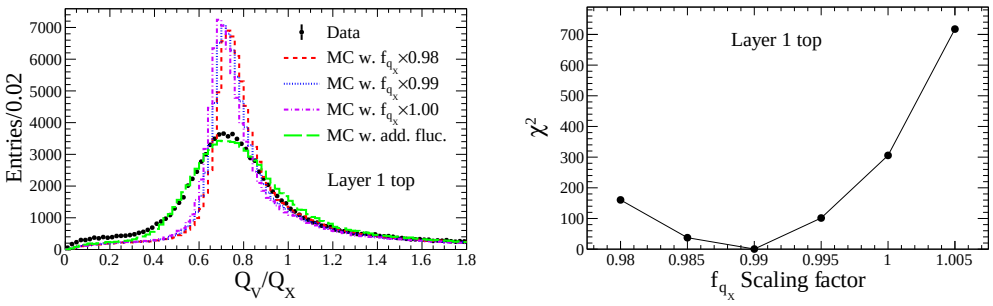

Figure 6. Left: charge sharing between X and V-cluster for data and MC samples on layer 1 top, where the dots with error bars represent the data, the red dashed lines, blue dot lines, purple dot-dashed lines the MC with a $f_{q\mathrm{X}}$ scaled by 0.98, 0.99, 1.0, respectively, and the green long-dashed lines the MC with additional charge fluctuation. Right: the χ^2 of the charge sharing peak position between data and MC as a function of $f_{q\mathrm{X}}$ scaling factor on layer 1 top.

The left plot of figure 6 shows the charge sharing between X and V-cluster for data and MC samples produced with different $f_{q\mathrm{X}}$ scaling factors on layer 1 top. The shift in the peak position of the charge sharing for MC with respect to data is small in this example, while the difference in the width is significant and it is connected strongly to the underestimated charge fluctuation in simulation which is tuned later, as described in the next section. The peak position of the charge sharing is estimated by a Gaussian fit. The χ^2 for the difference in peak position between data and MC as a function of the $f_{q\mathrm{X}}$ scaling factor is shown in the right plot of figure 6 for layer 1 top. To minimize the difference between data and MC in the peak position of the charge sharing, the charge fractions in X-view $f_{q\mathrm{X}}$ in simulation are scaled by 0.99, 1.025, 1.11, and 1.095 on layer 1 top, layer 1 bottom, layer 2 top, and layer 2 bottom, respectively. There is a small difference in the $f_{q\mathrm{X}}$ scaling factor between the top and the bottom parts of the same layer, while a significant difference between the two layers, mainly related to that the stereo angle between X and V strips is different between layers.

6.3 Charge fluctuation

For a better agreement of the width of the charge sharing between data and MC, the charge from simulation needs to be tuned by imposing an additional fluctuation. The additional charge fluctuation for a firing strip is assumed to obey a Gaussian function, where the width σ_q is assumed to depend only on the charge measured by the strip.

To consider the charge dependence of σ_q, the X-cluster charge is divided into several intervals. In each interval, the additional fluctuation in the Gaussian shape is sampled for the MC strip charge to reproduce the $Q_\mathrm{V}/Q_\mathrm{X}$ distributions. The left plot in figure 7 shows the charge sharing in the charge interval $0 < Q_\mathrm{X} < 40$ fC for data and the MC with different additional charge fluctuations on the layer 1 top. The χ^2/ndf of the charge sharing between data and MC is calculated for different additional charge fluctuations σ_q as shown the middle plot in figure 7. By minimizing the χ^2/ndf of the $Q_\mathrm{V}/Q_\mathrm{X}$ distributions between data and MC, a proper σ_q is found out in each interval. As the charge in V-view is smaller than in X-view, the relative fluctuation in charge sharing has a larger

2023 JINST 18 P05027

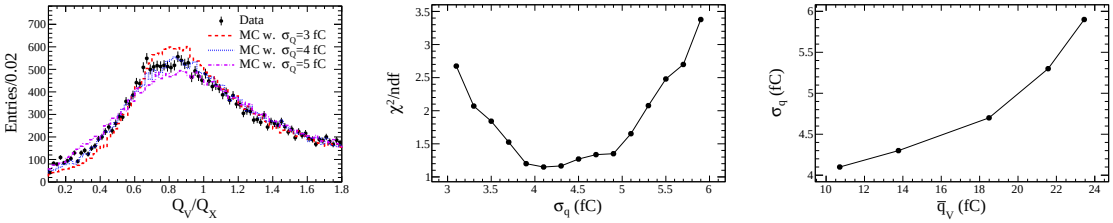

Figure 7. Charge sharing for data and MC within the charge interval $0 < Q_X < 40$ fC (left), χ^2/ndf of the charge sharing between data and MC as a function of the additional charge fluctuation σ_q (middle), and the extracted additional charge fluctuation as a function of the averaged charge of V-strip $\bar{q}_V$ (right).

contribution from V-view. The average strip charge in V-view $\bar{q}_V$ is calculated in each interval. Then the σ_q as a function of $\bar{q}_V$ is extracted as shown in the right plot of figure 7. These charge dependent Gaussian functions are used as a sampling model in E-branch for both X and V-views to reproduce the charge fluctuation in simulation. The Q_V/Q_X distribution for MC with the additional charge fluctuation agrees with the data as shown in the left plot of figure 6.

6.4 Electron diffusion

The cluster size (the number of strips in a cluster) distribution is affected by many factors, including micro-sectors, gain, charge sharing, thresholds, and electrons diffusion. As most of the factors are determined or tuned with other more relevant configurations or distributions, the electron diffusion becomes the last factor which can be tuned to adjust the cluster size simulation effectively.

For an electron drifting across a gap, the transverse position spread due to the diffusion effect is simulated by sampling a Gaussian function [10]. The width σ_{diffu} is scaled to produce MC samples. The cluster size distributions for data and MC with different σ_{diffu} scaling factors on layer 1 top are shown in the left plots of figure 8, where the χ^2 test is also performed. The right two plots of figure 8 shows the χ^2/ndf of cluster size distribution between data and MC as a function of the σ_{diffu} scaling factor on layer 1 top. A value of about 1.3 is found as the diffusion scaling factor minimizing the difference in cluster size distribution between data and MC, and is consistent between different views and half-layers as shown in table 1.

Table 1. Scaling factor for the diffusion width σ_{diffu} in simulation obtained by minimizing the difference in cluster size distribution between cosmic-ray data and MC.

	Layer 1 top	Layer 1 bottom	Layer 2 top	Layer 2 bottom
X-view	1.4	1.2	1.3	1.3
V-view	1.3	1.1	1.3	1.2

7 Comparison of cosmic-ray data and simulation

With all the previous tuning, the 2D-cluster charge, charge sharing, X-cluster and V-cluster charge distributions for data and MC are shown in figure 9. The consistency is good in general. This also indicates that the tuning order is rationally considered as the latter tuning changes only slightly the distributions which have been previously tuned.

2023 JINST 18 P05027

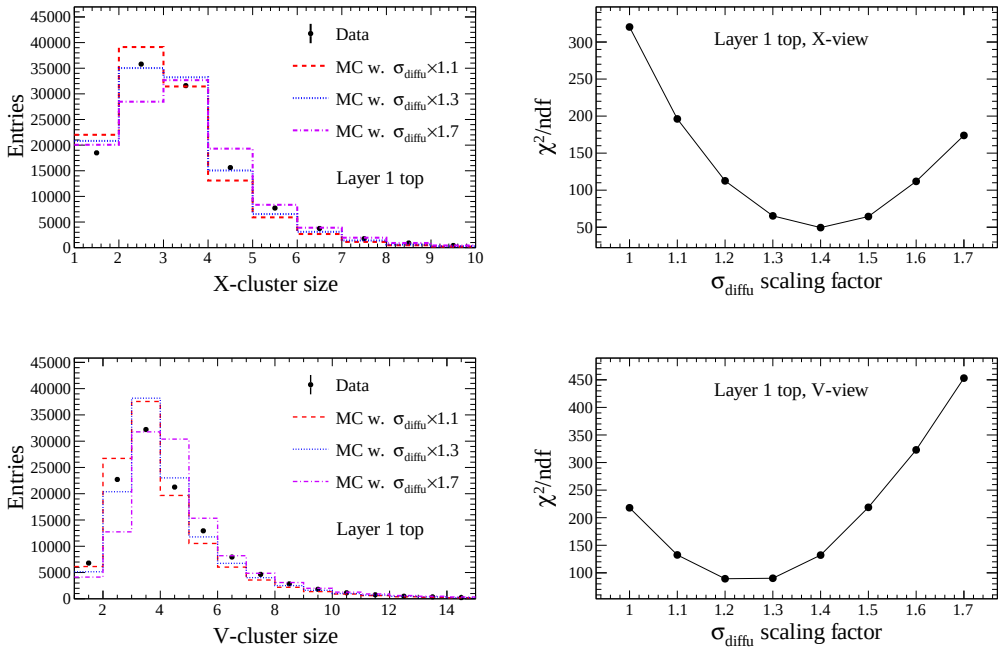

Figure 8. Left: X (top) and V (bottom) cluster size distribution on layer 1 top for data and MC with different σ_{diffu} scaling factors. Right: χ^2/ndf of X (top) and V (bottom) cluster size distributions between data and MC as a function of σ_{diffu} scaling factor.

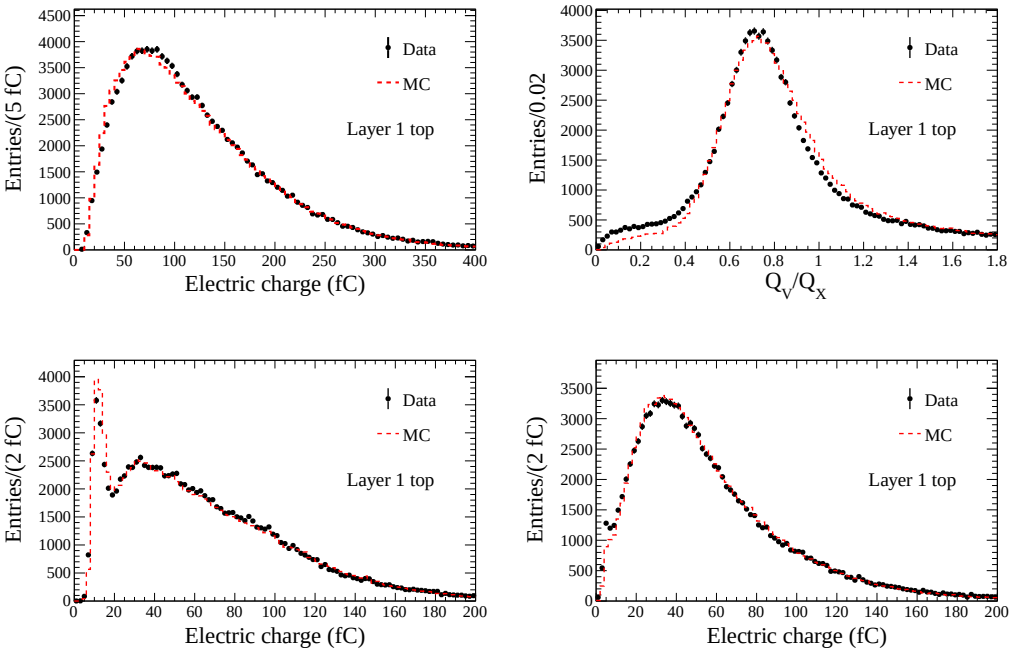

Figure 9. 2D-cluster charge (top left), charge sharing (top right), X-cluster charge (bottom left), and V-cluster charge (bottom right) distributions for comic-ray data and MC produced by the improved CGEM simulation. All the plots are for the layer 1 top of the CGEM.

2023 JINST 18 P05027

8 Conclusion and plan

By implementing the electronics response functions, together with the previously implemented CGEM digitization model including ionization, multiplication, diffusion and induction, a complete CGEM response simulation is now operational. Based on the comparison of cosmic-ray data acquired by the two layers of the CGEM detectors and MC, the micro-sector effect from GEM foils is simulated; the key parameters in the CGEM simulation are tuned in the following order: gain, charge sharing, charge fluctuation and electron diffusion, by minimizing the difference between data and MC. A general agreement between the cosmic-ray data and the MC is achieved with the improved CGEM simulation.

After all the three layers of CGEM are assembled and installed into the BESIII, more cosmic-ray data and large statistics of electron-positron collision data are going be collected and used to perform more extensive study to further improve the CGEM simulation.

Acknowledgments

This work is supported in part by National Natural Science Foundation of China (NSFC) under Contracts Nos. 12275297, 12275296, 12175259; National Key R&D Program of China under Contract No. 2020YFA0406304; the European Commission in the RISE Project 645664-BESIIICGEM, RISE-MSCA-H2020-2014 and in the RISE Project 872901-FEST, H2020-MSCA-RISE-2019.

References

[1] BESIII collaboration, *Design and construction of the BESIII detector*, *Nucl. Instrum. Meth. A* **614** (2010) 345 [arXiv:0911.4960].

[2] Q. Qin, L. Ma, J. Wang and C. Zhang, *Status and Performance of BEPCII*, *Conf. Proc. C* **100523** (2010) WEXMH01.

[3] BESIII collaboration, *Future Physics Programme of BESIII*, *Chin. Phys. C* **44** (2020) 040001 [arXiv:1912.05983].

[4] M.Y. Dong et al., *Aging effect in the BESIII drift chamber*, *Chin. Phys. C* **40** (2016) 016001 [arXiv:1504.04681].

[5] A. Amoroso et al., *A cylindrical GEM detector with analog readout for the BESIII experiment*, *Nucl. Instrum. Meth. A* **824** (2016) 515.

[6] F. Sauli, *GEM: A new concept for electron amplification in gas detectors*, *Nucl. Instrum. Meth. A* **386** (1997) 531.

[7] I. Balossino, *Operation and readout of the CGEM inner tracker*, *Nucl. Instrum. Meth. A* **1041** (2022) 167311 [arXiv:2205.11095].

[8] Z.Y. Deng et al., *Object-oriented BESIII detector simulation system*, *High Energy Phys. Nucl. Phys.* **30** (2006) 371.

[9] GEANT4 collaboration, *GEANT4 — a simulation toolkit*, *Nucl. Instrum. Meth. A* **506** (2003) 250.

[10] J.-Y. Zhao et al., *Digitization modeling of a CGEM detector based on Garfield++ simulation*, *Radiat. Detect. Technol. Meth.* **4** (2020) 174.

2023 JINST 18 P05027

[11] A. Amoroso et al., *The CGEM-IT readout chain*, 2021 *JINST* **16** P08065 [arXiv:2105.08979].

[12] M. Alexeev et al., *Triple GEM performance in magnetic field*, 2019 *JINST* **14** P08018 [arXiv:1908.06253].

[13] A.Q. Guo et al., *Track-based alignment for the BESIII CGEM detector in the cosmic-ray test*, *Nucl. Instrum. Meth. A* **1050** (2023) 168172 [arXiv:2211.01101].

[14] O.C. Allkofer, K. Carstensen and D.W. Dau, *The absolute cosmic ray muon spectrum at sea level*, *Phys. Lett. B* **36** (1971) 425.

[15] A. Dar, *Atmospheric Neutrinos, Astrophysical Neutrons, and Proton-Decay Experiments*, *Phys. Rev. Lett.* **51** (1983) 227.

[16] I.B. Smirnov, *Modeling of ionization produced by fast charged particles in gases*, *Nucl. Instrum. Meth. A* **554** (2005) 474.

[17] T. Zerguerras, B. Genolini, V. Lepeltier, J. Peyré, J. Pouthas and P. Rosier, *Single electron response and energy resolution of a Micromegas detector*, *Nucl. Instrum. Meth. A* **608** (2009) 397 [arXiv:0901.2882].

[18] R. Brun and F. Rademakers, *ROOT: An object oriented data analysis framework*, *Nucl. Instrum. Meth. A* **389** (1997) 81.

[19] N.D. Gagunashvili, χ^2 *test for comparison of weighted and unweighted histograms*, in proceedings of the *PHYSTAT (2005): Statistical Problems in Particle Physics, Astrophysics and Cosmology*, Oxford, U.K., 12–15 September 2005, Imperial College Press, London, U.K. (2006), pp. 191–192.

[20] N.D. Gagunashvili, *Comparison of weighted and unweighted histograms*, physics/0605123.

2023 JINST 18 P05027